Article

Journal of
Biomedical Nanotechnology
Vol. 14, 994–1008, 2018
www.aspbs.com/jbn

Combining Photodynamic Therapy and Chemotherapy: Improving Breast Cancer Treatment with Nanotechnology

Natalia Maria Candido[1], Maryanne Trafani de Melo[2], Leonardo Pereira Franchi[2], Fernando Lucas Primo[3], Antônio Cláudio Tedesco[2], Paula Rahal[1], and Marília Freitas Calmon[1,*]

[1]*Department of Biology, Institute of Bioscience, Language and Literature and Exact Science—IBILCE/UNESP, São José do Rio Preto, SP, 15054-000, Brazil*
[2]*Department of Chemistry, Faculty of Philosophy, Sciences and Letters of Ribeirão Preto—FFCLRP/USP, Ribeirão Preto, SP, 14040-900, Brazil*
[3]*Department of Bioprocess and Biotechnology, Faculty of Pharmaceutical Sciences of Araraquara—FCF/UNESP, Araraquara, SP, 14800-903, Brazil*

Nanomedical approaches are the major transforming factor in cancer therapies. Based on important previous works in the field of drug delivery nanomaterials, recent years have brought a broad array of new and improved intelligent nanoscale platforms that are suited to deliver drugs. In this context, the purpose of this study was to investigate the action of different nanoemulsions designed to encapsulate chloroaluminum phthalocyanine, a hydrophobic photosensitizer used in photodynamic therapy, and doxorubicin, a well-known chemotherapeutic agent used to treat aggressive breast cancer cells. The mean nanostructured system size ranged from 170.8 to 181.0 nm, and the nanoemulsions presented spherical morphology. All formulations exhibited negative zeta potential values (−68.7 to −75.0 mV) and suitable polydispersity values (0.20 to 0.28), explaining their colloidal stability up to three months. Murine breast cancer cells (4T1) were incubated with nanoemulsions for three hours at various concentrations and were subjected to cell viability tests to find the concentration dependence profile. Thereafter, the *in vitro* phototoxic effect was evaluated in the presence of the visible laser light irradiation. Less than 10% of 4T1 viable cells were observed when photodynamic therapy and chemotherapy were combined at a 1.0 $J \cdot cm^{-2}$ laser light dose with 1.0 μM phthalocyanine and 0.5 μM doxorubicin. The cell death assay and cell cycle arrest analysis confirmed the therapy efficiency demonstrating an increase in the apoptosis rate and in the cell cycle arrest on G2. Additionally, 15 genes related to apoptosis and 25 target genes of anti-cancer drugs were overexpressed. Four genes related to apoptosis and four target genes of anti-cancer drugs were downregulated in 4T1 cells after treatment with nanoemulsion with phthalocyanine and doxorubicin associated with photodynamic therapy. Thus, the nanoemulsions loaded with phthalocyanine and doxorubicin presented appropriate physical stability, improved photophysical properties, and remarkable activity *in vitro* to be considered as promising formulations for photodynamic therapy and chemotherapeutic use in breast cancer treatment.

KEYWORDS: *Breast Cancer, Nanoemulsion, Chloroaluminum Phthalocyanine, Doxorubicin, Photodynamic Therapy, Chemotherapy.*

INTRODUCTION

Breast cancer is the second most frequently diagnosed cancer worldwide and the leading cause of cancer death in the female population.[1,2] Breast cancer mortality rates remain high in Brazil, although it is considered a relatively good prognosis cancer whether diagnosed and treated timely. Additionally, survival is lower among women with a more advanced stage at diagnosis. Considering the whole spectrum and diversity of the population, the 5-year relative survival rate is 99% for localized disease, 85% for regional disease, and 26% for distant-stage disease.[3] Demonstrating its great medical concern, 57,960 new cases of breast cancer were expected in 2016 with an estimated risk of 56.20 cases per 100,000 Brazilian women.[4]

Generally, breast cancer is treated with surgery, radiotherapy, and chemotherapy, which are complex therapeutic resources considered invasive and potentially capable of promoting serious short- and/or long-term side effects.[5]

*Author to whom correspondence should be addressed.
Email: macal131@gmail.com
Received: 18 May 2017
Accepted: 6 February 2018

1550-7033/2018/14/994/015 doi:10.1166/jbn.2018.2558

Furthermore, there are unsatisfactory aesthetic results that, consequently, imply social and psychological impairment of the patient due to mutilations originated from the breast resection.[6–8] For all the reasons mentioned above, other therapeutic designs and new protocols are sought to reverse the poor life quality and relieve the collateral damage, improving the conventional and current treatment strategies.

In this context, photodynamic therapy (PDT) is presented as a promising approach for various oncological diseases.[9–15] The technique involves the topical or systemic administration of a photosensitizer followed by illumination of the tumor with visible light in a wavelength range matching the absorption spectrum of the photosensitizer.[16–18] The PDT efficacy can be improved using photosensitizer molecules that strongly absorb red light above 650 nm, where tissue exhibits optimal transparency. Thus, several new classes of potential sensitizers for PDT have been developed; among these, phthalocyanines have been found to be highly promising because of their high absorbance coefficient in the region of 650–680 nm.[19, 20]

Phthalocyanines can be chelated with various metals, usually aluminum and zinc because these diamagnetic metals enhance their phototoxicity.[21] Chloroaluminum phthalocyanine (ClAlPc) is a photosensitizer with adequate photophysical properties for PDT.[22, 23] Unfortunately, ClAlPc is insoluble in water and biologically compatible solvents, rendering its systemic administration problematic and restricting possible medical applications.[22] To overcome this limitation, phthalocyanines have been associated with different nanostructured systems, such as nanoemulsions.[24]

PDT can also be used either before or after chemotherapy, radiotherapy or surgery without compromising these therapeutic modalities. None of the clinically approved photosensitizers accumulate in the cells' nuclei, limiting DNA damage that could be carcinogenic or lead to the development of resistant clones. Moreover, the adverse effects of chemotherapy or radiation are absent, and radio- or chemoresistance do not imply sensitivity to PDT.[25] Thus, an interesting approach is to combine two therapeutic modalities, such as chemotherapy and photodynamic therapy, to enhance the treatment efficacy and take advantage of each care handling method.

For this, anthracyclines, particularly doxorubicin (DOX), is the cornerstone of chemotherapy for breast cancer. However, the use of this agent is limited by dose-related cardiotoxicity, myelosuppression and a range of toxicities such as alopecia and fatigue, which, while not life-threatening, reduce the therapeutic index of conventional anthracyclines in the palliative setting, especially for older patients.[26, 27] Thus, much attention has been focused on the design of an alternative delivery system for DOX, and the emergence of nanotechnology has been beneficial to this particularly research.

Nanoemulsions (NEs) are capable of delivering high concentration of chemotherapy drugs to cancerous tissues without affecting cells and organs in the systemic circulation. Formulations of lipophilic anticancer drugs in oil/water NEs have proven to be highly promising because they offer the advantages of a unique size, drug solubilization, passive targeting by enhanced permeability and retention effect, controlled drug release, and further modification for long circulation *in vivo*, escape from reticuloendothelial system, and tumor-specific targeting.

Therefore, in this study, we developed and characterized nanoemulsions of oil-water to contain chloroaluminum phthalocyanine (ClAlPc) to deliver doxorubicin (DOX), using its nanotechnological properties in photobiological studies and an *in vitro* model to assess the PDT response in the biological environment.

EXPERIMENTAL REAGENTS AND INSTRUMENTS

Preparation of the Nanoemulsions

Four different nanostructured systems were synthesized: nanoemulsions containing chloroaluminum phthalocyanine (NEPc), nanoemulsions with doxorubicin (NEDOX), nanoemulsions containing both drugs (NEPcDOX) and empty NEs without any drugs. Nanoemulsions were obtained using a spontaneous emulsification process as previous described by Tabosa do Egito[28] with some modifications.[28]

Briefly, for the NEPc, the organic phase (acetone) was prepared containing medium-chain-triglycerides, natural soy phospholipids (Liposoid S100, Lipid Co, Brazil) and ClAlPc (Sigma-Aldrich, USA), at 55 °C. Subsequently, this organic solution was added into the aqueous phase containing an anionic surfactant, and poloxamer 188 (Sigma-Aldrich, USA) under magnetic stirring. Finally, the organic solvent was fully removed by rota-evaporation under reduced pressure at 60 °C.

Regarding NEDOX, the nanoemulsion was similarly prepared, except for the addition of the photosensitizer, and doxorubicin was added to the aqueous phase instead. Additionally, for NEPcDOX, both drugs were added to the final formulation. The formulations without drugs were prepared under the same conditions, to be used as a reference for subsequent tests. All samples were prepared under aseptic conditions and in the absence of contaminants and chemical interference.

Characterization of the Nanoemulsions

All of the prepared nanoemulsions were characterized for size, homogeneity, shelf-life stability (supplementary material), residual charge and morphology. The average diameter and the polydispersity index (PdI) of the colloidal formulations were determined by photon correlation spectroscopy at 25 °C with a 173 scattering angle in a Nano Zetasizer® ZS analyzer (Malvern PCS Instruments, UK).

Samples were obtained by diluting 10 μL of nanoemulsion in 1 mL of ultrapure water. The zeta potential of the NEs was measured by electrophoretic mobility also using a Zetasizer® Nano ZS equipment. The analyzes were conducted at 25 °C, and samples were appropriately diluted (1/100) in 0.1 M KCl solution. The values are shown as the means ± standard error of three different batches of each colloidal dispersion.

For the morphology analyses, the images of the formulations were acquired at 25 °C, without the need to cover the sample, using a Scanning Probe Microscope model machine SPM-9600 (Shimadzu, Japan) and SPM Online software provided by Shimadzu. The samples of each formulation (5.0 μL) were deposited on a mica surface, spread and dried on a drop of argon jet. The images were obtained using the intermittent contact mode with a cantilever 124 mm in length, operating at a resonance frequency with a range of 324–369 KHz, a stiffness of 34–51 N/m and constant force. Dimensional results were processed using the software from the microscope, and at least ten images of each sample were analyzed to ensure reproducible results.

Drug Encapsulation Efficiency

Encapsulation efficiency (EE%) of AlClP and Dox in nanoemulsions were determined by the fluorescence method previously validated for AlClPc and Dox as described by Siqueira-Moura et al.[29] The content of AlClP and Dox were analyzed with fixed excitation at 615 nm and 480 nm (Fluorolog-3 Spectrofluorimeter, Horiba, New Jersey, USA) and fixed emission at 674 nm and 560 nm respectively. The free AlClPc content and free Dox were determined by evaluating the unincorporated drug present in a clear ultrafiltrate obtained by separating the aqueous phase using an ultrafiltration/ultracentrifugation procedure (Ultracel Microcon YM-100, Millipore, Ireland) at 12857× g for 1 h at 4 °C (Eppendorf, Centrifuge 5810 R, Hamburg, Germany). The encapsulation efficiency for calculation as follows Eq. (1):

$$E.E.\% = TPc - LPc/TPct \times 100 \quad (1)$$

Where, TPc represents a total drug concentration in the nanoemulsion formulation, LPc is the concentration of free drug present non-supernatant of the nanoemulsion sample subjected to ultracentrifugation/ultrafiltration for total separation of the aqueous phase and TPt is the theoretical concentration of drug.

Determination of the Singlet Oxygen Quantum Yield

The detection of singlet oxygen was performed by an indirect spectrophotometric method. 1,3-Diphenyl-benzofuran (DPBF) was used as a probe.[30] Samples were prepared immediately at the time of the experiment. Solutions containing the samples were prepared in 2.0 mL of acetonitrile, so that the absorption in the 660 nm region of these solutions were close to 0.3. A stock solution of DPBF (8.00 mmol/L) was also prepared 10.0 μL of the stock solution of DBPF was transferred to the 2.0 mL solution of the sample with acetonitrile, and the initial electronic absorption spectrum of that solution was measured. The solution was irradiated at 20 mW at a wavelength of 660 nm in a quartz cuvette, with constant magnetic stirring for 1-second time intervals. At each irradiation, the absorption spectrum was measured again. The experiment was performed in triplicate, at room temperature and dark room. The laser used was the Eagle diode laser, and the absorption spectra were obtained through a UV-visible GE Ultrospec 7000 spectrophotometer. After extraction with DMSO, absorption measurements were performed in acetonitrile medium on a GE Ultrospec 7000 spectrophotometer in the 300 to 800 nm wavelength range. The fluorescence emission spectra were performed on a Horiba Jobin Ivon-Spex Fluorolog-3 spectrofluorimeter (New Jersey, USA), adjusted with a fixed excitation at 615 nm and fluorescence emission in the 650 and 750 nm range.

Cell Culture

The murine breast cancer cell line (4T1) acquired from ATCC was cultured in Roswell Park Memorial Institute medium (RPMI1640) (GIBCO-BRL, Life Technologies, USA) supplemented with 10% fetal bovine serum (FBS) (Cultilab, Brazil), 100 U/mL penicillin (GIBCO-BRL, Life Technologies, USA), and 100 μg/mL streptomycin (GIBCO-BRL, Life Technologies, USA). The cells were maintained in a humidified 5% CO_2 incubator and a constant temperature of 37 °C.

Cytotoxicity Assay

Cytotoxicity was assessed using the MTT assay, which is a nonradioactive, colorimetric assay. The 4T1 cells were seeded into 96-well plates (10^4 cells) (TPP, Switzerland) previously for 24 hours and were incubated at 37 °C in a chamber with 5% CO_2.

The cells were treated with the nanoemulsions NEPc (0.5, 1.0 and 2.0 μM), NEDOX (0.25, 0.5 and 1.0 μM), NEPcDOX (1.0 μM ClAlPc and 0.5 μM DOX), and the empty NE (no drug) was used as the control of the experiment. All NEs were incubated for three hours, and then, the incubated solution was removed and the cell culture medium was added to the cells. The assay was performed after 24, 48 and 72 hours of incubation with the nanoemulsions, associated or not. After these periods, the medium containing nanoemulsions was replaced with 100 μL of MTT (Sigma-Aldrich, USA) (1 mg/mL) diluted in RPMI1640 medium, and the plates were incubated for 30 minutes at 37 °C. Finally, the supernatant solution was aspirated, and 100 μL/well of DMSO added. The absorbances were read using a plate reader (Safire 2, Tecan Group Ltd., Austria) at a wavelength of 570 nm. All experiments were performed in triplicate, and in three independent events.

The obtained values were normalized with control cells that were subjected to the same test conditions and without the addition of nanoemulsions under study, expressed as a cell viability percentage value with the standard error, and calculated according to Eq. (2) as follows:

$$\text{Viable cells} = (\text{mean OD sample/mean control OD}) \times 100\% \quad (2)$$

Where O.D. indicates optical density.

Cellular Uptake of the Nanoemulsions

Chloroaluminum phthalocyanine and doxorubicin are naturally fluorescent in the visible spectrum. To analyze the intracellular uptake of encapsulated ClAlPc and DOX nanoemulsions, 3×10^4 4T1 cells were plated on glass coverslips allocated at the bottom of 24-well plates (TPP, Switzerland), allowing growth at subconfluent levels. Next, the cells were incubated with 1.0 μM NEPc, 0.5 μM NEDOX, or 1.0 μM ClAlPc/0.5 μM DOX in NEPcDOX (selected concentrations from the MTT assay previously described in item 2.4). Untreated cells, without NEs, were used as a negative control.

Following three hours of incubation, cells were washed with PBS and were fixed with 4% paraformaldehyde for 20 minutes at room temperature. Subsequently, the cells were washed again with PBS and then were incubated for five minutes with PBS containing 100 mM glycine (Sigma-Aldrich, USA) and were permeabilized with Triton X-100 0.1% diluted in PBS (Sigma-Aldrich, USA) for seven minutes at room temperature. Next, the coverslips were washed with PBS and mounted on glass slides, using ProLong® reagent (Life Technologies, USA) containing DAPI (4′,6-diamidino-2-phenylindole).

The slides were observed under a confocal microscope TCS-SP8 (Leica Microsystems, Germany). ClAlPc was detected at the emission/excitation of 610/675 nm, DOX was detected at 480/560 nm, and DAPI was evaluated at 360/460 nm.

Cell Viability and Phototoxicity

Next, the effect of photodynamic therapy in the 4T1 cell line in the presence of nanoemulsions was studied. Based on the cytotoxicity studies, the working conditions for the application of PDT were established. Given that the concentration of 1.0 μM chloroaluminum phthalocyanine and the concentration of 0.5 μM doxorubicin encapsulated showed low toxicity in the dark, these values were adopted for the tests with photostimulation. Furthermore, from the cell viability studies in the absence of the laser, we proposed two forms of treatment of breast cancer to be combined in the presence of the laser: the first one using the nanoemulsion containing ClAlPc associated with DOX (NEPcDOX), and the second using ClAlPc separately from DOX, which was based on combined treatment in which the NEPc incubation is followed by incubation with NEDOX 24 hours later.

After confluency was established in the cultivation bottles, the cells were trypsinized and seeded at a density of 10^4 cells in 24-well plates. The next day, the culture medium containing 10% FBS was replaced with medium containing 3% FBS and nanoemulsions (NEPc or NEPcDOX), followed by incubation for three hours at 37 °C, 5% CO_2 and protected from light. Next, the incubated solution was removed, and then the cells were washed with PBS, and phenol red-free culture medium was added (Cultilab, Brazil) without FBS for the application of monochromatic laser light at 675 nm. For both treatments, photoactivation was carried out following incubation with the photosensitizer drug in nanoemulsion (NEPc or NEPcDOX).

Cells were irradiated using a laser Eagle 2 W-630 nm (Quantum Tech, Brazil) operating at 60 mW power with irradiation times adjusted to obtain energy densities of 100, 500 and 1000 $mJ \cdot cm^{-2}$. After irradiation, the medium without phenol red was replaced with culture medium containing 10% FBS, and cells were again incubated for 24 hours in the case of treatment with NEPcDOX. However, for the combined therapy, a subsequent step was added after photoactivation of the cells incubated with NEPc. After 24 hours, the cells were subjected to incubation for three hours with NEDOX. After replacing this solution with nanoemulsion, the cell culture medium containing 10% FBS was added to the cells, which were incubated for the next 24 hours until analysis.

Finally, the standard cell viability assay MTT was performed. In this experiment, the control was established as cells without photosensitization and irradiation. The results were expressed as the mean values of the cell viability ±standard error of experiments in triplicate and in three independent events.

Cell Death Upon Treatment

To evaluate the effect of photodynamic therapy on possible cell death, the 4T1 cells were seeded at a density of 4×10^4 in 24-well plates. The following day, incubation and treatment protocols proceeded as described in item cell viability and phototoxicity. However, cell death analysis was performed 24 hours after the end of treatments only, because significant differences could not be found between the times of 24, 48 and 72 hours from the cell viability assay. Thus, 24 hours after the end of treatment with the associated nanoemulsion (NEPcDOX) or combined therapy (NEPc and NEDOX), at the concentrations of the drugs previously selected by the MTT assay, viable, apoptotic and necrotic cells were determined.

The supernatant culture medium was removed from each well, and the plate was transferred to the properly identified tubes. Subsequently, the cells were trypsinized and homogenized, and they were also transferred to the tubes. Subsequently, the tubes were centrifuged for five

minutes at 4 °C and 1000 rpm. Part of the supernatant was discarded, leaving 100 μL of the initial solution. To each sample was added 100 μL of Guava Nexin® reagent (Millipore, USA), which contains Annexin V-PE and 7-AAD, and the tubes were incubated for 20 minutes at room temperature in the dark. Finally, the contents of the tubes were transferred to 96-well round-bottom plates (Corning, USA), and the analysis was performed for 5,000 events using a Guava Easycheck 8HT flow cytometer (Millipore, Germany).

The results were analyzed using the software of the equipment and were expressed as mean values of the percentage of viable cells (negative for staining with Annexin V and 7-AAD), early apoptotic cells (positive only for Annexin V), late apoptotic cells (positive for Annexin V and 7-AAD) and necrotic cells (positive only for 7-AAD) ±standard error of the experiments in triplicate.

Cell Cycle Evaluation

Similarly, cell death was assessed resulting from the treatments, and possible cell cycle arrest was also evaluated. For this, 4T1 cells were seeded at a density of 4×10^4 in 24-well plates. The incubation and treatment protocols were followed as described in item cell viability and Phototoxicity, and the analyses were performed only 24 hours after the end of treatments.

The protocol for the removal of the culture medium plates, trypsinization of the cells and centrifugation of the tubes was carried out similarly to that in Section Cellular Uptake of the Nanoemulsions. Subsequently, the supernatant was completely discarded, and the cells were fixed with 200 μL of cold 70% ethanol. The samples were incubated at 4 °C for 24 hours and then centrifuged for five minutes at 4 °C and 1000 rpm. The supernatant was discarded, and the cells were washed with PBS and incubated for 20 minutes in the dark with 200 μL of Guava Cell Cycle® reagent (Millipore, USA), containing propidium iodide. For analysis, the contents of the tubes were transferred to 96-well round-bottom plates (Corning, USA), and 5,000 events were acquired using the Guava EasyCyte 8HT flow cytometer (Millipore, Germany).

The results were analyzed using GuavaSoft™ software and were expressed as the mean values of the percentage of cells in the G1 interphase, G2 or subG1 ±standard error of experiments in triplicate.

RNA Isolation, cDNA Synthesis and Amplification

Total RNA from 4T1 cells after six hours of treatment with NEPcDOX associated with photodynamic therapy and 4T1 cells without treatment were isolated using the RNeasy mini kit following the manufacturer's instructions (Qiagen, Germany). Total RNA (2 μg) from each group of 4T1 cells was reverse transcribed using the first-strand cDNA synthesis kit (Qiagen, Germany), following the manufacturer's instructions.

PCR Arrays

The amplified cDNA was then diluted with nuclease-free water and was added to the RT² qPCR SYBR green Master Mix (Qiagen, Germany). The experimental cocktail (25 μL) was added to each well of the mouse Cancer Drug Targets RT Profiler PCR array (Qiagen, Germany) or mouse Apoptosis RT Profiler PCR array (Qiagen, Germany). Real-time PCR was performed on the Applied Biosystems 7300 Real-Time PCR System (Applied Biosystems, USA) and was used for SYBR green detection using the following thermal profile: segment 1–1 cycle: 95 °C for 10 minutes, segment 2–40 cycles: 95 °C for 15 seconds followed by 60 °C for one minute, segment 3 (dissociation curve) –95 °C for one minute, 55 °C 30 seconds, and 95 °C for 30 seconds. The RT2 Profiler PCR array Data Analysis version 3.5 (Qiagen, USA) (http://pcrdataanalysis.sabiosciences.com/pcr/arrayanalysis.php) was used to analyze the differential expression of genes between the two groups of 4T1 cells (treated and untreated).

Statistical Analysis

The data were analyzed using GraphPad Prism 5 software, and the statistical significance of differences between the results was determined by analysis of variance (ANOVA) followed by post-test Tukey t-test for multiple comparisons. The probability of $p < 0.05$ was considered as significant in this study.

RESULTS AND DISCUSSION

Physicochemical Properties and Morphology of the Nanoemulsions

The formulations were characterized by determination of the particle size (hydrodynamic diameter), polydispersity index and zeta potential by scattered light in the absence and presence of the photosensitizer (ClAlPc) and chemotherapeutic compound (DOX).

The results in Table I indicated a distribution of particles with an average size of 170.8 nm (±1.0), 178.0 nm (±2.0), 181 nm (±0.7) and 180.1 nm (±0.7) for empty NEs, NEPc, NEDOX, and NEPcDOX, respectively. These results demonstrated no significant influence of the photosensitizer agent and chemotherapeutic drug nanoencapsulation on the size of colloidal particles.

Table I. Size, polydispersity and zeta potential for the nanoemulsions in the presence or absence of the photosensitizer ClAlPc and chemotherapeutic agent DOX.

Nanoemulsion	Size (nm)	Polydispersity	Zeta potential (mV)
Empty NE	170.8±1.0	0.25	−69.0±0.20
NEPc	178.0±2.0	0.24	−72.5±0.20
NEDOX	181.0±0.7	0.20	−68.7±0.15
NEPcDOX	180.1±0.7	0.28	−75.0±0.12

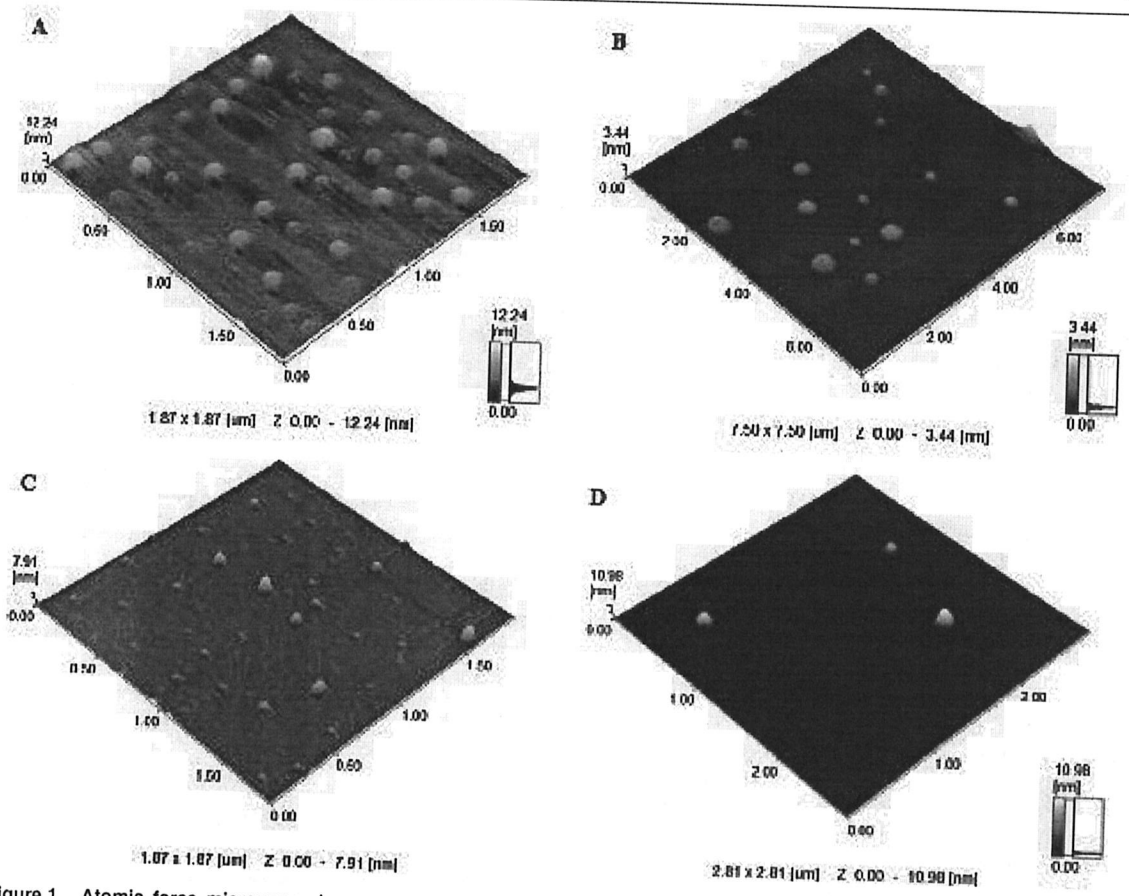

Figure 1. Atomic force microscopy images producing a three-dimensional view of (A) empty NE, (B) NEPc (C) NEDOX and (D) NEPcDOX spherical nanostructures spread on mica. Scan sizes are described below each NE.

The nanometer design introduced in the pharmaceutical technology a wide range of options to improve the encapsulation of different compounds in these systems, in which conventional therapies often present limitations due to undesirable effects in the administration of drugs.[31–33]

It was noted that the average particle size is in the desired operating range, and the polydispersity index remained in the range of 0.2 to 0.28 (Table I), demonstrating a low consistent heterogeneity with the expected distribution type, a finding that is in accordance with a previous report.[34]

The surface charges formed by ionic interaction with counter ions in solution were evaluated based on the zeta potential measurement, which is the theoretical electric potential between the aqueous environment and a diffused region of the opposite predominant load surface in the Stern layer. The results in Table I indicated that the zeta potential of the systems are of the order of −69.0 mV (±0.20), −72.5 mV (±0.20), −68.7 mV (±0.15) and −75.0 mV (±0.12), for the empty NE, NEPc, NEDOX, and NEPcDOX, respectively. These values showed a mostly negative surface potential, the balance result of the surface charges of poloxamers and phospholipids. The results were within the stability range for this physicochemical parameter, which covers results higher than +30 mV and smaller than −30 mV, since in this potential region has greater stability, balance results between repulsive and attractive phenomena of the loads, namely, stability factors governed by electrostatic.[35]

Atomic force microscopy is a technique with a resolution of 1–100 Å that allows the visualization of particles without sample handling. Using this technique, it is possible to characterize features of the particle such as shape and structure.[36,37] In the three-dimensional analysis, shown in Figure 1, all the nanoemulsions showed a spherical shape and low polydispersity, demonstrating that most of the particles had similar sizes. These findings corroborate those results from particle size determined by the diffusion method using photon correlation spectroscopy.

Table II. Encapsulation efficiency rate (E.E.%) of AlClPc in various formulations of nanoemulsions.

Formulations	E.E. %
NEPcAlCl	100
NEDOX	96
NEPcAlClDOX	83

Drug Encapsulation Efficiency

The Table II shows the encapsulation efficiency for all formulations. The means of E.E. were between 83% and 100%, that is, all formulations were able to encapsulate the drugs satisfactorily, even when associated. It was observed a slight decrease in the encapsulation efficiency of AlClPc when associated with DOX, but without statistically significant difference.

Lipophilic compounds can be encapsulated at rates of 70% or more.[38] The encapsulation efficiency observed for the formulations studied is in accordance with that described in the literature.

Determination of the Singlet Oxygen Quantum Yield

As shown in Table III and in Figures 2 and 3, it was possible to obtain the quantum yield values of singlet oxygen production for the samples studied. The phthalocyanines metallized with zinc and aluminum in their free form presented values of 0.56 and 0.61 respectively, confirming their high potential for the production of this reactive species in homogeneous organic medium. The AlClPc encapsulation strategy induced a slight decrease in yield to 0.41, resulting in a reduction of only 33%. The yields obtained for phthalocyanine are in agreement with the literature.[39] The NEPc were consistent with that found in the literature.[40] The polymeric chemical environment characteristic of a colloidal drug delivery system may affect the diffusional process of this reactive species. However the value found is sufficient for induction of biological processes requirements for the photodynamic effect. Thus, it may be suggested that the NEPc formulation has potential for use in future procedures that seek photodynamic evaluation for treatment of tumor models *in vivo* assays.

Table III. Singlet oxygen quantum yield by the relative 1,3-diphenyl benzofuran method (DPBF).

Sample	Quantum yields (Φ_Δ)
ZnPc*	0.56
AlClPc*	0.61
NE/AlClPc**	0.41

Notes: *Photosensitizers free in acetonitrile medium; **AlClPc after entrapment in nanoemulsion.

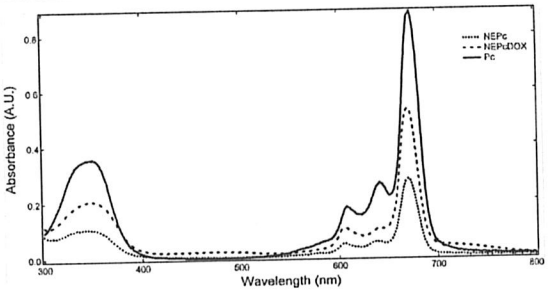

Figure 2. UV-visible spectra for different samples: Pc = free phthalocyanine in organic medium; NEPc = phthalocyanine-containing nanoemulsion; NEPcDOX = phthalocyanine-containing nanoemulsion + doxorubicin.

Cell Viability

The main property of an ideal photosensitizer applied to PDT is its low level of dark toxicity—i.e., the photosensitizer drug should be non-toxic in the absence of light irradiation.[41–43] Therefore, to determine the best dose-response of nanoemulsions that would not affect 4T1 cells in the absence of photoactivation, the MTT assay was carried out for formulations containing a photosensitizer drug or chemotherapeutic agent.

As shown in Figure 4, after incubation times of 24, 48 and 72 hours, there was no significant cytotoxic effect on the cell line in the absence of light stimulation and at different concentrations of NEPc ($p > 0.05$). Cell viability remained high, similar to percentages found in the experimental control (4T1 cells incubated with only culture medium) (Fig. 2). For analyses involving the formulation NEDOX, it was found that it causes a significant decrease in cell viability at a concentration above 0.5 μM for all analyzed times ($p < 0.05$), with a reduction in the viable cell percentage to 75.0% (±2.14) compared with untreated cells (Fig. 5). Because the empty NE showed very low

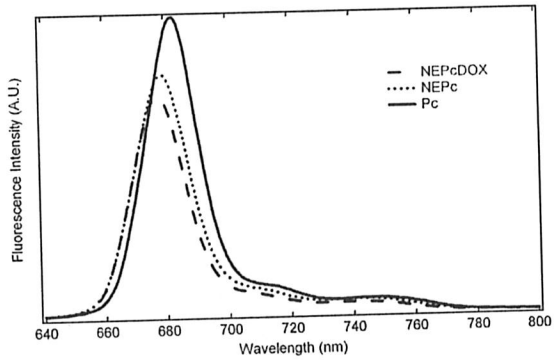

Figure 3. Standardized fluorescence spectra for different samples: Pc = free phthalocyanine in organic medium; NEPc = phthalocyanine-containing nanoemulsion; NEPcDOX = phthalocyanine-containing nanoemulsion + doxorubicin. λ excitation = 615 nm; emission and excitation slits = 5/5 nm.

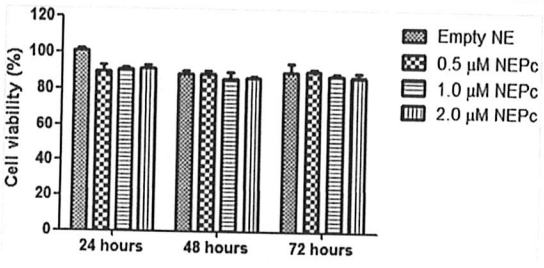

Figure 4. Cytotoxicity assay in the murine breast cancer cell line 4T1 incubated with nanoemulsions containing chloroaluminum phthalocyanine (NEPc) at different concentrations and without photoactivation. Nanoemulsions without the photosensitizer drug (empty NEs) were used as control. *Statistical significance $p < 0.05$ compared with negative control cells incubated with culture medium.

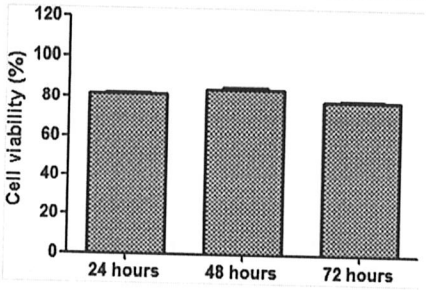

Figure 6. Cytotoxicity assay in 4T1 murine breast cancer cells incubated with NEPcDOX (containing 1.0 μM ClAlPc and 0.5 μM DOX) and without photoactivation. *Statistical significance of $p < 0.05$ compared with experimental control cells incubated with culture medium.

cytotoxicity ($p > 0.05$), we could testify, therefore, that the cell toxicity displayed in the trials are due to drug and not the reagents required for the synthesis of NEs, confirming the nanoemulsion biocompatibility (Figs. 4 and 5). These results agree with earlier research stating that polymeric nanoemulsions can be biocompatible with tissue and cells when they are synthesized from biocompatible or biodegradable materials.[38, 44]

Thus, the concentrations of 1.0 μM ClAlPc and 0.5 μM DOX were selected to use as safe doses to ensure the absence of toxicity due only to the formulations in subsequent experiments. To observe whether the association between the drugs could enhance the cell proliferation inhibition mechanism, the MTT assay was performed for 4T1 cells incubated with the formulation containing 1.0 μM ClAlPc associated with 0.5 μM DOX. In this assay, there was not cytotoxicity for NEPcDOX at the selected concentration for the times of 24, 48 and 72 hours ($p > 0.05$) (Fig. 6). Thus, the cell viability assays in the dark showed that the association of the photosensitizer and chemotherapeutic drugs may be used as a therapeutic modality for cancer cells studied at the experimental times (such as 24 hours). It is also worth to notice that it would not be desirable to use the formulation NEPcDOX in higher concentrations for both drugs whose could cause toxicity by itself, in the absence of light stimulation.

The biocompatibility, combined with adequate biodistribution, leads to results that favor the use of these processes in protocols *in vivo*. A low cytotoxicity is directly related to the reduction of side effects caused after systemic, topical or transdermal administration of the formulations. Therefore, it was found that the formulations have suitable biocompatibility, allowing the continuity of further studies with laser application, discarding any interfering or cell death in the absence of light stimulus.

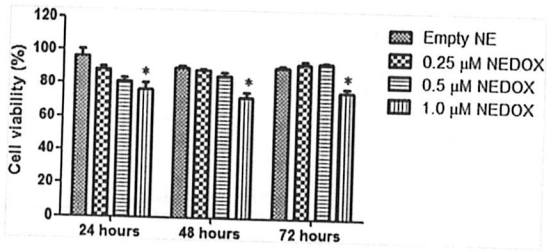

Figure 5. Cytotoxicity assay in the murine breast cancer cell line 4T1 incubated with different concentrations of nanoemulsions containing doxorubicin (NEDOX) and without photoactivation. Nanoemulsions without the chemotherapeutic agent (empty NEs) were used as the control. *Statistical significance of $p < 0.05$ compared with negative control cells incubated with culture medium.

Cell Uptake of the Nanoemulsions

After three hours of incubation, the analysis by confocal microscopy confirmed the internalization of ClAlPc derived from NEPc (Fig. 7). It was possible to observe the intracellular distribution profile of the photosensitizer being completely located in the cytoplasmic region of the 4T1 cells, as noted in the figures marked in red and encircling the nuclei stained blue by the DAPI fluorescent label. The results are in accordance with other studies, suggesting the cell uptake was kept at the cytoplasmic level, once ClAlPc internalization was concentrated in the cytosol of cancerous and non-cancerous cells.[45, 46] The incorporation of ClAlPc by the cytoplasm could be explained by the characteristic of the photosensitizer to preferentially accumulate in organelles such as lysosomes and mitochondria, for example.[47, 48] These results further suggest that the cell internalization profile of the NEs is similar to that proposed for liposomes-which are endocytosed and undergo the action of lysosomes-, and other organelles. The nanoparticles would then be endocytosed, and the polymer chain would be degraded for later release of the drug.[49, 50]

It was also possible to qualitatively verify the ClAlPc internalization (at a concentration of 1.0 μM) when associated with DOX (at a concentration of 0.5 μM) (Fig. 7). A plausible explanation for there being no alteration in the permeation when the drugs were associated is that the

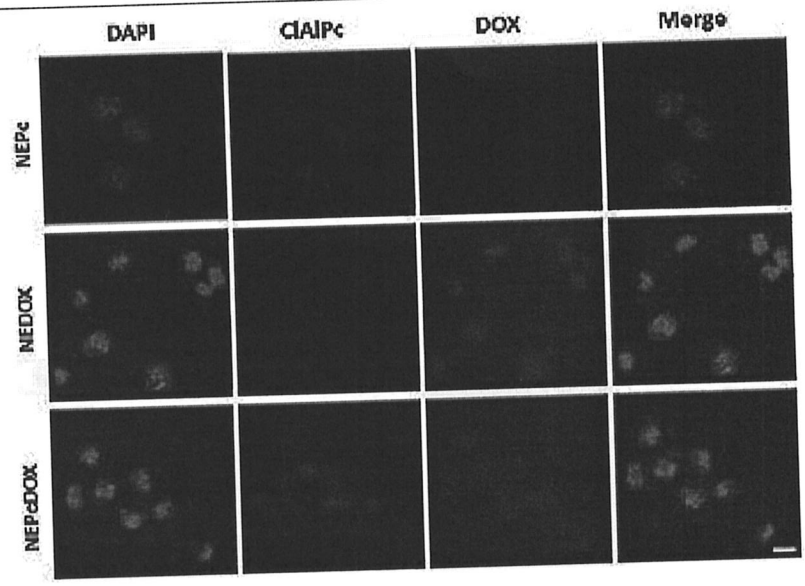

Figure 7. Confocal laser scanning microscopy images of *in vitro* uptake of NEPc, NEDOX and NEPcDOX by 4T1 cells. Photomicrographs were taken after three hours of incubation with the formulations. Chloroaluminum phthalocyanine (ClAlPc) is marked in red, green represents doxorubicin (DOX), and nuclei are labeled with DAPI in blue. Scale bar: 10 μm.

mechanism of action in cells would not be changed by the NE binding to the cell membrane. Thus, DOX would not compete for the internalization of the ClAlPc compound.

The efficient internalization of DOX (marked in green) by the 4T1 cells was displayed when incubated with NEDOX and NEPcDOX (Fig. 7). Because the therapeutic activity of doxorubicin is achieved by the interleaving process with DNA, inhibiting topoisomerase II, and preventing the synthesis of DNA and RNA, the intranuclear localization of this chemotherapeutic agent was expected.[51]

Effects of the Phototoxicity on 4T1 Cells

Once the ideal scanning time (24 hours), the biocompatible drug concentrations of nanoemulsions (1.0 μM ClAlPc and 0.5 μM DOX) and an efficient cell internalization mechanism (ClAlPc located in the cytoplasm and DOX in the nucleus) were verified, phototoxicity tests were performed to determine the most effective treatment against breast cancer cells. For this, two therapeutic approaches were developed involving the photoactivation: the first used a formulation containing ClAlPc associated with DOX, and the second involved a 'two-step' treatment in which a nanoemulsion containing only ClAlPc was first used followed by a formulation containing only DOX. For both proposed therapies, laser treatment at different increasing light doses was used, varying the energies among 100, 500, and 1000 mJ $\cdot$ cm^{-2}.

The phototoxic effect is closely related to the photosensitizer concentration, visible light dose applied and tissue oxygen level. To assess cell damage due to the irradiation dose, different light doses were applied as described above. A gradual decrease in the cell viability was observed due to the increased energy dose applied to the studied cell line (Fig. 8). A light dose of 1000 mJ $\cdot$ cm^{-2} exerted a maximum significant toxic effect on 4T1 cells ($p < 0.001$). The minimum cell viability reached was 10.3% for the treatment with NEPcDOX (Fig. 8(A)) and 3.3% for the 'two-step' treatment (NEPc and NEDOX, Fig. 8(B)). This represents an excellent phototoxic effect of ClAlPc associated with another drug; consequently, PDT was significantly effective in all of the suggested approaches. In a less significant manner, there are other reports that observed a similar or inferior therapeutic effect of PDT for the different types of cancers as well as for breast cancer cells.[52–55]

Thus, the phototoxicity studies indicated that photodamage was dependent on the energy dose applied to the 4T1 cell line (Fig. 8). The results showed that ClAlPc associated with DOX, both used at low concentrations and in combination with irradiation with visible light of low intensity, induced a substantial decrease in cell viability, indicating that these new formulations are a potential alternative for breast cancer treatment, and a great incentive for future studies with PDT application.

Apoptotic cell death is known as "programmed or active" controlled by intracellular and extracellular factors, resulting in a sequence of morphological, biochemical and energetic changes-, more specifically, cell shrinkage, nuclear condensation and fragmentation. Necrosis, on the other hand, is an aggressive, rapidly cell degeneration,

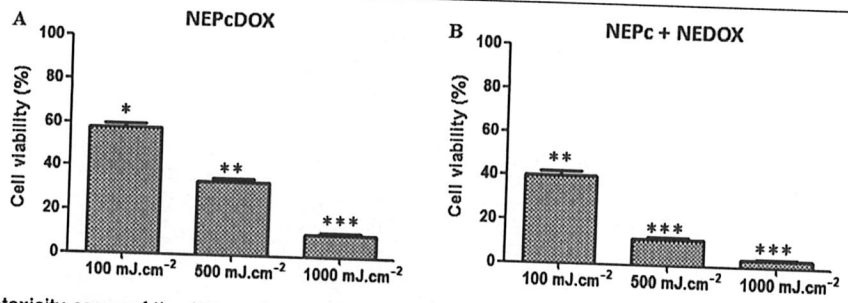

Figure 8. Phototoxicity assay of the 4T1 murine breast cancer cell line incubated with (A) NEPcDOX (containing 1.0 μM ClAlPc and 0.5 μM DOX) and (B) the combined test with 1.0 μM NEPc under photoactivation of 100, 500 or 1000 mJ·cm^{-2} followed by 0.5 μM NEDOX. *Statistical significance of $p < 0.05$ compared with experimental control cells incubated with culture medium.

characterized by cytoplasmic swelling, organelle destruction and disruption of the plasma membrane, leading to the release of intracellular content and inflammation.[56,57]

The main factors that determine the type of cell death after the application of PDT are the cell type, type of photosensitizing agent and subcellular localization and light dose applied during treatment.[58] The scientific literature reports that PDT application leads to cell death mostly by apoptosis. Hydrophobic photosensitizing drugs are located in the mitochondrial membrane, and this subcellular localization of the photoactive molecule is primordial in the photodynamic process because it determines the site of primary damage. Therefore, photosensitizing compounds located in mitochondria rapidly induce apoptosis.[47]

The analyses of cell death assay involving NEPcDOX or NEPc/NEDOX therapeutic approaches are similar to those observed in the literature and described below, with an increase in the amount of apoptotic cells after the use of a laser at a dose of 1000 mJ·cm^{-2}, compared with that NEPcDOX before and after photoactivation ($p < 0.05$) (Fig. 9(A)). Additionally, according to the results, there was a decrease in the viable cell number that was less remarkable in the combined therapy ($p > 0.05$) (Fig. 9(B)). Finally, necrotic cells (7-AAD stained) have not undergone significant change over the test ($p > 0.05$), thereby demonstrating that cell death resulting from PDT was substantially characterized by apoptosis.

A crucial factor for development and tumor growth is the balance between proliferation and cell death. Because the decrease in cell viability can be directly related to increased apoptosis/necrosis and cell cycle arrest, studies involving all of these parameters can be useful for predicting tumor behavior in the initial phase of carcinogenesis. Thus, to verify why there was a significant decrease in cell viability (MTT assay) without a remarkable increase in cell death (flow cytometry), cell cycle analysis was performed for the 4T1 cell line treated with the two therapeutic approaches proposed.

A very small amount of cells was observed in G1 and S in all situations, particularly after photoactivation, but the cell number was slightly higher when they were incubated with only NEPcDOX (Fig. 10). There was a significant increase in the percentage of cells in subG1 ($p < 0.05$) following treatment with a dose of 1000 mJ·cm^{-2} for both NEPcDOX and NEPc/NEDOX therapies, reaching 95% and 80% of cells, respectively (Fig. 10). Therefore, the decrease in cell viability is directly related to the increase in cells in subG1. In addition, cell cycle data for NEPcDOX without photoactivation corroborated the MTT cytotoxicity assay results, indicating that almost 23% of cells were in subG1 (referring to cell viability of approximately 80% after 24 hours analysis) (Fig. 10).

Due to doxorubicin cell cycle arrest in G2, there was an increased amount of cells in the checkpoint when cells were treated with the combined therapy but in the absence of photoactivation (Fig. 10(B)), featuring a repair mechanism damage by the cells. In addition to the mechanisms mentioned above, DOX may exert its antitumor activity

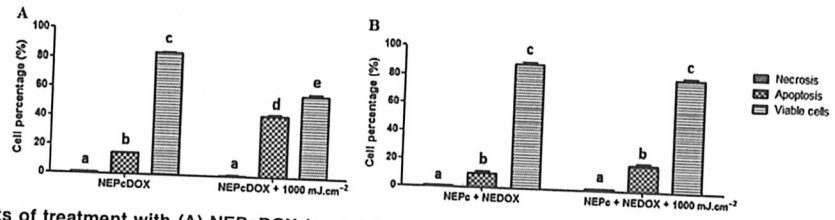

Figure 9. Effects of treatment with (A) NEPcDOX (containing 1.0 μM ClAlPc and 0.5 μM DOX) and (B) the combined test with 1.0 μM NEPc, with or without photoactivation of 1000 mJ·cm^{-2}, followed by 0.5 μM NEDOX on the percentage of 4T1 cells positively stained for Annexin V-PE and/or 7-AAD. Necrosis, apoptosis (initial and late), and viable cells are highlighted. Different letters indicate significant difference between groups according to each type of treatment ($p < 0.05$).

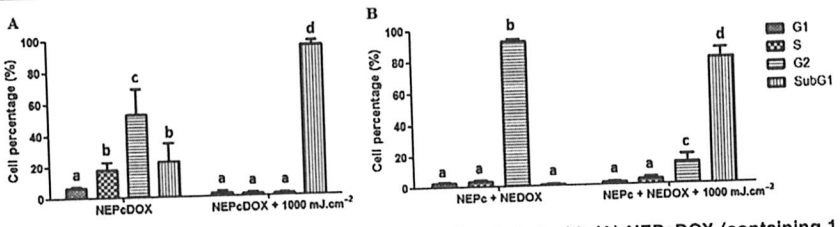

Figure 10. Cell cycle test in the murine breast cancer cell line 4T1 incubated with (A) NEPcDOX (containing 1.0 μM ClAlPc and 0.5 μM DOX) and (B) the combined test with 1.0 μM NEPc, under photoactivation 1000 mJ·cm^{-2} or not, followed by 0.5 μM NEDOX. Cells in G1, S, G2 and subG1 are shown in the graph. Different letters denote the significant difference between groups for each treatment ($p < 0.05$).

by intercalation into the DNA, leading to the inhibition of macromolecular synthesis by binding to DNA and alkylation, by cross bridges and DNA intrastrands, interference in the separation process of the double-stranded DNA by interfering with the activity of the helicase, all mechanisms directly related to cell cycle control.[59,60]

Therefore, ClAlPc and PDT would act as facilitators for cell death, and DOX would act on a second front of attack being responsible for cell cycle arrest in G2. This would be the most powerful strategy that we assessed in this work, proving that combining the two therapies is the most successful option for cancer treatment and against 4T1 cell line.

Expression of Apoptosis-Associated Genes and Target Genes of Anti-Cancer Drugs in 4T1 Cells Treated with NEPcDOX Associated with Photodynamic Therapy

To identify possible apoptosis signaling pathways and target genes of anti-cancer drugs, the changes in the gene expression profile of the 4T1 cells without treatment and after treatment with NEPcDOX associated with photodynamic therapy were analyzed by RT2 Profiler PCR arrays. Target genes of anti-cancer drugs with differential expression between 4T1 cells are listed in Table IV.

cdk1 and *cdk7* genes, which presented low expression in 4T1 cells after treatment, are members of the Ser/Thr family and are essential for the G1/S and G2/M phase transitions of the cell cycle. Cyclin-dependent kinase control cell proliferation by regulating cell cycle entry and passage and dysregulation of this family, either by increased expression or mutation, is often associated with breast cancer.[61,62] Therefore, cyclin-dependent kinases, mainly CDK7, have been considered as important targets for anti-cancer treatments.[63] The *birc5* gene, which also presented low expression in the treated 4T1 cells, is a member of the apoptosis inhibitor family, which negatively encodes regulatory proteins that prevent cell death by apoptosis. This gene is expressed in several primary tumors and has low expression in normal differentiated tissues.[64] Studies have shown that inhibitors of *birc5* inhibited proliferation and induced apoptosis in gastric cancer cells and necrosis in renal cancer cells.[65,66] Another gene that presented low expression in the treated 4T1 cells was *figf*, also known as *VEGFD*, is a member of the vascular endothelial growth factor family and is active in angiogenesis, lymphangiogenesis and endothelial cell growth.[67] In addition, some studies have indicated that *VEGFD* overexpression is associated with a poor prognosis by promoting lymphatic metastasis in breast cancer, lung adenocarcinoma, colorectal carcinoma and gastric adenocarcinoma.[68–70]

Table IV. Differential expression of target genes of anti-cancer drugs in 4T1 cells after treatment with NEPcDOX associated with photodynamic therapy.

Gene symbol	Fold regulation	*p*-value
Atf2	−2,0139	0,000759
Aurka	−3,1095	0,000001
Aurkb	−2,3295	0,000018
Bcl2	−2,3241	0,000007
Birc5	−2,5257	0,000006
Cdk1	−2,214	0,000097
Cdk7	−3,0314	0,000014
Cdk8	−2,042	0,000013
Ctsd	−2,4005	0
Esr1	−2,042	0,000008
Hdac2	2,3457	0,000011
Hsp90b1	−3,387	0,000006
Kras	−2,4116	0
Nras	−184,8229	0,012325
Parp1	−2,3674	0,00001
Parp2	−2,555	0,000005
Pdgfrb	−3,0525	0,000541
Pik3c2a	−3,8637	0,000004
Pik3c3	−2,2243	0,000002
Plk1	−3,234	0
Plk4	−2,434	0
Prkca	−2,2191	0,000013
Tert	−2,0186	0,000001
Top2a	−2,3511	0,000003
Top2b	−2,214	0,000008
Gusb	−3,891	0,000001
Kdr	5,3765	0
Pgr	3,8194	0,000003
Plk3	4,103	0,000037
Rhob	7,551	0

Table V. Differential expression of genes related to apoptosis in 4T1 cells after treatment with NEPcDOX and those associated with photodynamic therapy.

Gene symbol	Fold regulation	*p*-value
Aifm1	−3.1456	0.000129
Api5	−2.3511	0.000011
Bcl2	−2.3241	0.000007
Bcl2l11	−2.042	0.000011
Birc5	−2.8219	0
Bnip2	−2.8415	0.000005
Dad1	−2.0139	0
Dapk1	−2.3729	0.000104
Fasl	−2.1886	0.000013
Mapk1	−2.1685	0.000003
Naip2	−2.1287	0.000028
Ripk1	−2	0
Tnfrsf10b	−2.1189	0.000001
Xiap	−3.0738	0.000006
Gusb	−4.0093	0.000001
Cd70	3.6385	0.000005
Gadd45a	2.4794	0
Il10	5.278	0.000001
Tnf	6.0769	0.000002

On the other hand, the *Plk3* and *Rhob* genes, for example, are highly expressed in the treated 4T1 cells and are also involved in important cellular processes. *PLK3*, a cytokine-inducible kinase, prevents cell cycle progression and tumorigenesis. In most studies, deregulated expression of *Plk3* results in cell cycle arrest, apoptosis and growth suppression.[71,72] *RhoB* is a tumor suppressor because its expression is decreased in several tumor cell types and its expression promotes apoptosis in epithelial cancer cells and fibroblasts.[73–75]

The genes related to apoptosis with differential expression in treated 4T1 cells are listed in Table V. One of the genes with low expression in treated 4T1 cells is *Bcl2*, which encodes a mitochondrial membrane protein that blocks the death of some cells.[76,77] The genes *Dad1*, *Api5*, *Naip2* and *Xiap* also showed low expression, such that the gene *Dad1* is a negative regulator of cell death, The *Api5* gene is an apoptosis inhibitor whose expression prevents apoptosis after growth factor deprivation by suppressing the apoptosis-induced E2F1 transcription factor, the *Naip2* gene belongs to a family of apoptosis-inhibiting proteins, that can inhibit procaspase 9, and the gene *Xiap* belongs to a family of apoptosis inhibitor proteins, inhibiting at least two members of the caspase family, caspase-3 and caspase-7.[78–81]

One of the genes that presented high expression in treated 4T1 cells is *tnf*, which belongs to a superfamily that mediates the extrinsic apoptosis pathway. *TNF* is produced by cells of the immune system, including activated natural killer cells, T cells and activated monocytes/macrophages and various cells, such as fibroblasts.[82] TNF/TNFR signaling is involved in several cellular processes such as apoptosis, cell differentiation and differentiation.[83]

CONCLUSION

In summary, empty NE, NEPc, NEDOX, and NEPcDOX formulations can be synthesized with desirable morphology, homogeneous diameter distribution and optimal residual charge, indicating that there was no formation of agglomerates or physico-chemical destabilization of samples during their shelf life.

The nanoemulsions exhibited biocompatibility with the evaluated murine breast cancer cells, because there was no significant cytotoxicity at the doses and selected incubation times. Furthermore, the nanostructured systems containing chloroaluminum phthalocyanine and/or doxorubicin were effective for the internalization into target cells. Therefore, the *in vitro* trials demonstrated that ClAlPc, once encapsulated in nanoemulsion, could generate a good photodynamic response leading to cell death, and showing great potential to act as photosensitizer in a photodynamic therapy system. Regarding DOX, it can contribute to cytotoxicity and cell cycle arrest when delivered efficiently to cancer cells. Therefore, we suggest that the innovative NEPcDOX should be considered an effective material system for chemotherapeutic drug delivery and a PDT inductor in antitumor therapy, and the combined approach should be considered as a promising form of treatment for breast cancer that triggers cell apoptosis and alters the expression of target genes to anticancer drugs, as well as that of genes related to cell death and cell cycle regulation. For this, the efficiency of the suggested treatments should be further studied *in vivo*.

Disclosure

The authors report no conflicts of interest in this study.

Acknowledgments: The authors acknowledge the financial support of CAPES and FAPESP (Process number 2015/16660-5).

REFERENCES

1. R. L. Siegel, K. D. Miller, and A. Jemal, Cancer statistics, 2016. *CA: A Cancer Journal for Clinicians* 66, 7 (2016).
2. A. P. Cecilio, E. T. Takakura, J. J. Jumes, J. W. Dos Santos, A. C. Herrera, V. J. Victorino, and C. Panis, Breast cancer in Brazil: Epidemiology and treatment challenges. *Breast Cancer (Dove Med Press)* 7, 43 (2015).
3. A. N. N. Howlander, M. Krapcho, K. Bishop, and A. Cronin, SEER Cancer Statistics Review, 1975–2013, National Cancer Institute, Bethesda, MD (2015).
4. INCA, Estimativa 2016: Incidência de câncer no Brasil (2015).
5. A. Di Leo, G. Curigliano, V. Dieras, L. Malorni, C. Sotiriou, C. Swanton, A. Thompson, A. Tutt, and M. Piccart, New approaches for improving outcomes in breast cancer in Europe. *Breast* 24, 321 (2015).
6. S. N. Razdan, V. Patel, S. Jewell, and C. M. McCarthy, Quality of life among patients after bilateral prophylactic mastectomy: A systematic review of patient-reported outcomes. *Quality of Life Research: An International Journal of Quality of Life Aspects of Treatment, Care and Rehabilitation* 25, 1409 (2016).

7. P. E. Bidstrup, J. Christensen, B. G. Mertz, N. Rottmann, S. O. Dalton, and C. Johansen, Trajectories of distress, anxiety, and depression among women with breast cancer: Looking beyond the mean. *Acta Oncol.* 54, 789 (**2015**).
8. J. R. Schubart, M. Emerich, M. Farnan, J. S. Smith, G. L. Kauffman, and R. B. Kass, Screening for psychological distress in surgical breast cancer patients. *Annals of Surgical Oncology* 21, 3348 (**2014**).
9. R. J. Skyrme, A. J. French, S. N. Datta, R. Allman, M. D. Mason, and P. N. Matthews, A phase-1 study of sequential mitomycin C and 5-aminolaevulinic acid-mediated photodynamic therapy in recurrent superficial bladder carcinoma. *BJU International* 95, 1206 (**2005**).
10. A. Kubler, C. Niziol, M. Sidhu, A. Dunne, and J. A. Werner, Analysis of cost effectiveness of photodynamic therapy with Foscan (Foscan-PDT) in comparison with palliative chemotherapy in patients with advanced head-neck tumors in Germany. *Laryngo-Rhino-Otologie* 84, 725 (**2005**).
11. L. E. Rhodes, M. de Rie, Y. Enstrom, R. Groves, T. Morken, V. Goulden, G. A. Wong, J. J. Grob, S. Varma, and P. Wolf, Photodynamic therapy using topical methyl aminolevulinate versus surgery for nodular basal cell carcinoma: Results of a multicenter randomized prospective trial. *Archives of Dermatology* 140, 17 (**2004**).
12. C. Hur, N. S. Nishioka, and G. S. Gazelle, Cost-effectiveness of photodynamic therapy for treatment of Barrett's esophagus with high grade dysplasia. *Digestive Diseases and Sciences* 48, 1273 (**2003**).
13. H. Kato, Photodynamic therapy for lung cancer—A review of 19 years' experience. *Journal of Photochemistry and Photobiology B, Biology* 42, 96 (**1998**).
14. B. J. Park, K. H. Choi, K. C. Nam, A. Ali, J. E. Min, H. Son, H. S. Uhm, H. J. Kim, J. S. Jung, and E. H. Choi, Photodynamic anticancer activities of multifunctional cobalt ferrite nanoparticles in various cancer cells. *J. Biomed. Nanotechnol.* 11, 226 (**2015**).
15. L. S. Bicalho, J. P. Longo, C. E. Cavalcanti, A. R. Simioni, A. L. Bocca, F. S. Mde, A. C. Tedesco, and R. B. Azevedo, Photodynamic therapy leads to complete remission of tongue tumors and inhibits metastases to regional lymph nodes. *J. Biomed. Nanotechnol.* 9, 811 (**2013**).
16. R. R. Allison and C. H. Sibata, Oncologic photodynamic therapy photosensitizers: A clinical review. *Photodiagnosis and Photodynamic Therapy* 7, 61 (**2010**).
17. Y. N. Konan, R. Gurny, and E. Allemann, State of the art in the delivery of photosensitizers for photodynamic therapy. *Journal of Photochemistry and Photobiology B, Biology* 66, 89 (**2002**).
18. P. Avci, S. S. Erdem, and M. R. Hamblin, Photodynamic therapy: One step ahead with self-assembled nanoparticles. *J. Biomed. Nanotechnol.* 10, 1937 (**2014**).
19. M. N. Sibata, A. C. Tedesco, and J. M. Marchetti, Photophysicals and photochemicals studies of zinc(II) phthalocyanine in long time circulation micelles for photodynamic therapy use. *European Journal of Pharmaceutical Sciences: Official Journal of the European Federation for Pharmaceutical Sciences* 23, 131 (**2004**).
20. Y. N. Konan, M. Berton, R. Gurny, and E. Allemann, Enhanced photodynamic activity of meso-tetra(4-hydroxyphenyl)porphyrin by incorporation into sub-200 nm nanoparticles. *European Journal of Pharmaceutical Sciences: Official Journal of the European Federation for Pharmaceutical Sciences* 18, 241 (**2003**).
21. M. D. P. Kluson, A. Kalaji, M. Karaskova, and J. Rakusan, Preparation, chemical modification and absorption properties of various phthalocyanines. *Research on Chemical Intermediates* 35, 13 (**2009**).
22. S. M. Nunes, F. S. Sguilla, and A. C. Tedesco, Photophysical studies of zinc phthalocyanine and chloroaluminum phthalocyanine incorporated into liposomes in the presence of additives. *Brazilian Journal of Medical and Biological Research* 37, 11 (**2004**).
23. M. S. Rocha, C. M. Lucci, J. P. Longo, P. D. Galera, A. R. Simioni, Z. G. Lacava, A. C. Tedesco, and R. B. Azevedo, Aluminum-chloride-phthalocyanine encapsulated in liposomes: Activity against naturally occurring dog breast cancer cells. *J. Biomed. Nanotechnol.* 8, 251 (**2012**).
24. G. B. Rodrigues, A. C. Tedesco, and G. U. Braga, *In vitro* photodynamic inactivation of cryptococcus neoformans melanized cells with chloroaluminum phthalocyanine nanoemulsion. *Photochem. Photobiol.* 88, 7 (**2012**).
25. P. Agostinis, K. Berg, K. A. Cengel, T. H. Foster, A. W. Girotti, S. O. Gollnick, S. M. Hahn, M. R. Hamblin, A. Juzeniene, D. Kessel, M. Korbelik, J. Moan, P. Mroz, D. Nowis, J. Piette, B. C. Wilson, and J. Golab, Photodynamic therapy of cancer: An update. *CA: A Cancer Journal for Clinicians* 61, 250 (**2011**).
26. C. F. Jehn, P. Hemmati, S. Lehenbauer-Dehm, S. Kummel, B. Flath, and P. Schmid, Biweekly pegylated liposomal doxorubicin (caelyx) in heavily pretreated metastatic breast cancer: A phase 2 study. *Clinical Breast Cancer* 16, 514 (**2016**).
27. R. E. Coleman, L. Biganzoli, P. Canney, L. Dirix, L. Mauriac, P. Chollet, V. Batter, E. Ngalula-Kabanga, C. Dittrich, and M. Piccart, A randomised phase II study of two different schedules of pegylated liposomal doxorubicin in metastatic breast cancer (EORTC-10993). *Eur. J. Cancer* 42, 882 (**2006**).
28. F. M. A. P. B. D. Tabosa Do Egito, New techniques for preparing submicronic emulsions: Application to amphotericin B. *STP Pharma Sciences* 4, 7 (**1994**).
29. M. P. Siqueira-Moura, F. L. Primo, A. P. Peti, and A. C. Tedesco, Validated spectrophotometric and spectrofluorimetric methods for determination of chloroaluminum phthalocyanine in nanocarriers. *Die Pharmazie* 65, 9 (**2010**).
30. L. M. Rossi, P. R. Silva, L. L. Vono, A. U. Fernandes, D. B. Tada, and M. S. Baptista, Protoporphyrin IX nanoparticle carrier: Preparation, optical properties, and singlet oxygen generation. *Langmuir: The ACS Journal of Surfaces and Colloids* 24, 12534 (**2008**).
31. R. Alvarez-Roman, A. Naik, Y. N. Kalia, R. H. Guy, and H. Fessi, Skin penetration and distribution of polymeric nanoparticles. *Journal of Controlled Release: Official Journal of the Controlled Release Society* 99, 53 (**2004**).
32. G. A. Hughes, Nanostructure-mediated drug delivery. *Nanomedicine: Nanotechnology, Biology, and Medicine* 1, 22 (**2005**).
33. J. Shim, H. Seok Kang, W. S. Park, S. H. Han, J. Kim, and I. S. Chang, Transdermal delivery of mixnoxidil with block copolymer nanoparticles. *Journal of Controlled Release: Official Journal of the Controlled Release Society* 97, 477 (**2004**).
34. C. S. de Paula, A. C. Tedesco, F. L. Primo, J. M. Vilela, M. S. Andrade, and V. C. Mosqueira, Chloroaluminium phthalocyanine polymeric nanoparticles as photosensitisers: Photophysical and-physicochemical characterisation, release and phototoxicity *in vitro*. *Eur. J. Pharm. Sci.* 49, 10 (**2013**).
35. W. Rungtiwa, S. Shobsngob, B. Oonkhanond, and S. Varavinit, Zeta potential (ζ) analysis for the determination of protein content in rice flour. *Starch-Stärke* 57, 6 (**2004**).
36. C. Preetz, A. Hauser, G. Hause, A. Kramer, and K. Mader, Application of atomic force microscopy and ultrasonic resonator technology on nanoscale: Distinction of nanoemulsions from nanocapsules. *European Journal of Pharmaceutical Sciences: Official Journal of the European Federation for Pharmaceutical Sciences* 39, 141 (**2010**).
37. M. A. Pereira, V. C. Mosqueira, J. M. Vilela, M. S. Andrade, G. A. Ramaldes, and V. N. Cardoso, PLA-PEG nanocapsules radiolabeled with 99mTechnetium-HMPAO: Release properties and physicochemical characterization by atomic force microscopy and photon correlation spectroscopy. *European Journal of Pharmaceutical Sciences: Official Journal of the European Federation for Pharmaceutical Sciences* 33, 42 (**2008**).
38. C. E. Mora-Huertas, H. Fessi, and A. Elaissari, Polymer-based nanocapsules for drug delivery. *International Journal of Pharmaceutics* 385, 113 (**2010**).
39. W. Spiller, H. Kliesch, D. Wöhrle, S. Hackbarth, B. Röder, and G. Schnurpfeil, Singlet oxygen quantum yields of different photosensitizers in polar solvents and micellar solutions. *Journal of Porphyrins and Phthalocyanines* 2, 145 (**1998**).

40. J. Ma, J. Y. Chen, M. Idowu, and T. Nyokong, Generation of singlet oxygen via the composites of water-soluble thiol-capped CdTe quantum dots-sulfonated aluminum phthalocyanines. *The Journal of Physical Chemistry B* 112, 4465 (2008).
41. K. Plaetzer, B. Krammer, J. Berlanda, F. Berr, and T. Kiesslich, Photophysics and photochemistry of photodynamic therapy: Fundamental aspects. *Lasers in Medical Science* 24, 259 (2009).
42. C. P. D. Bechet, C. Frochot, M. L. Viriot, F. Guillemin, and M. Barberi-Heyob, Nanoparticles as vehicles for delivery of photodynamic therapy agents. *Trends Biotechnol.* 26, 9 (2008).
43. A. P. Castano, T. N. Demidova, and M. R. Hamblin, Mechanisms in photodynamic therapy: Part one-photosensitizers, photochemistry and cellular localization. *Photodiagnosis and Photodynamic Therapy* 1, 279 (2004).
44. D. Moinard-Checot, Y. Chevalier, S. Briancon, H. Fessi, and S. Guinebretiere, Nanoparticles for drug delivery: Review of the formulation and process difficultics illustrated by the emulsion-diffusion process. *J. Nanosci. Nanotechnol.* 6, 2664 (2006).
45. L. B. de Paula, F. L. Primo, M. R. Pinto, P. C. Morais, and A. C. Tedesco, Combination of hyperthermia and photodynamic therapy on mesenchymal stem cell line treated with chloroaluminum phthalocyanine magnetic-nanoemulsion. *Journal of Magnetism and Magnetic Materials* 380, 4 (2015).
46. L. A. Muehlmann, B. C. Ma, J. P. F. Longo, M. D. F. Menezes, A. Santos, and R. B. Azevedo, Aluminum–phthalocyanine chloride associated to poly(methyl vinyl ether-co-maleic anhydride) nanoparticles as a new third-generation photosensitizer for anticancer photodynamic therapy. *International Journal of Nanomedicine* 9, 14 (2014).
47. D. Li, L. Li, P. Li, Y. Li, and X. Chen, Apoptosis of HeLa cells induced by a new targeting photosensitizer-based PDT via a mitochondrial pathway and ER stress. *OncoTargets and Therapy* 8, 703 (2015).
48. S.-M. M. P. A. Barbugli, E. M. Espreafico, and A. C. Tedesco, *In vitro* phototoxicity of liposomes and nanocapsules containing chloroaluminum phthalocyanine on human melanoma cell line. *J. Nanosci. Nanotechnol.* 10, 4 (2010).
49. L. A. Muehlmann, B. C. Ma, J. P. Longo, F. A. S. Mde, and R. B. Azevedo, Aluminum-phthalocyanine chloride associated to poly(methyl vinyl ether-co-maleic anhydride) nanoparticles as a new third-generation photosensitizer for anticancer photodynamic therapy. *Int. J. Nanomedicine* 9, 1199 (2014).
50. W. M. Sharman, J. E. van Lier, and C. M. Allen, Targeted photodynamic therapy via receptor mediated delivery systems. *Advanced Drug Delivery Reviews* 56, 53 (2004).
51. Y. Pommier, E. Leo, H. Zhang, and C. Marchand, DNA topoisomerases and their poisoning by anticancer and antibacterial drugs. *Chemistry and Biology* 17, 421 (2010).
52. P. A. Barbugli, C. P. Alves, E. M. Espreafico, and A. C. Tedesco, Photodynamic therapy utilizing liposomal ClAlPc in human melanoma 3D cell cultures. *Experimental Dermatology* 24, 970 (2015).
53. J. D. Meyers, Y. Cheng, A. M. Broome, R. S. Agnes, M. D. Schluchter, S. Margevicius, X. Wang, M. E. Kenney, C. Burda, and J. P. Basilion, Peptide-targeted gold nanoparticles for photodynamic therapy of brain cancer. *Particle and Particle Systems Characterization: Measurement and Description of Particle Properties and Behavior in Powders and Other Disperse Systems* 32, 448 (2015).
54. M. P. Siqueira-Moura, F. L. Primo, E. M. Espreafico, and A. C. Tedesco, Development, characterization, and photocytotoxicity assessment on human melanoma of chloroaluminum phthalocyanine nanocapsules. *Materials Science and Engineering C, Materials for Biological Applications* 33, 1744 (2013).
55. X. Wang, J. Hu, P. Wang, S. Zhang, Y. Liu, W. Xiong, and Q. Liu, Analysis of the *in vivo* and *in vitro* effects of photodynamic therapy on breast cancer by using a sensitizer, sinoporphyrin sodium. *Theranostics* 5, 772 (2015).
56. T. Luedde, N. Kaplowitz, and R. F. Schwabe, Cell death and cell death responses in liver disease: Mechanisms and clinical relevance. *Gastroenterology* 147, 765 (2014).
57. A. P. Castano, T. N. Demidova, and M. R. Hamblin, Mechanisms in photodynamic therapy: Part three-photosensitizer pharmacokinetics, biodistribution, tumor localization and modes of tumor destruction. *Photodiagnosis and Photodynamic Therapy* 2, 91 (2005).
58. A. C. Moor, Signaling pathways in cell death and survival after photodynamic therapy. *Journal of Photochemistry and Photobiology B, Biology* 57, 1 (2000).
59. G. Minotti, P. Menna, E. Salvatorelli, G. Cairo, and L. Gianni, Anthracyclines: Molecular advances and pharmacologic developments in antitumor activity and cardiotoxicity. *Pharmacological Reviews* 56, 185 (2004).
60. A. Buschini, P. Poli, and C. Rossi, Saccharomyces cerevisiae as an eukaryotic cell model to assess cytotoxicity and genotoxicity of three anticancer anthraquinones. *Mutagenesis* 18, 25 (2003).
61. M. Malumbres and M. Barbacid, Mammalian cyclin-dependent kinases. *Trends in Biochemical Sciences* 30, 630 (2005).
62. J. Bartkova, M. Zemanova, and J. Bartek, Expression of CDK7/CAK in normal and tumor cells of diverse histogenesis, cell-cycle position and differentiation. *International Journal of Cancer* 66, 732 (1996).
63. H. Patel, R. Abduljabbar, C. F. Lai, M. Periyasamy, A. Harrod, C. Gemma, J. H. Steel, N. Patel, C. Busonero, D. Jerjees, J. Remenyi, S. Smith, J. J. Gomm, L. Magnani, B. Gyorffy, L. J. Jones, F. Fuller-Pace, S. Shousha, L. Buluwela, E. A. Rakha, I. O. Ellis, R. C. Coombes, and S. Ali, Expression of CDK7, cyclin H, and MAT1 is elevated in breast cancer and is prognostic in estrogen receptor-positive breast cancer. *Clinical Cancer Research: An Official Journal of the American Association for Cancer Research* 22, 5929 (2016).
64. I. Tamm, Y. Wang, E. Sausville, D. A. Scudiero, N. Vigna, T. Oltersdorf, and J. C. Reed, IAP-family protein survivin inhibits caspase activity and apoptosis induced by Fas (CD95), Bax, caspases, and anticancer drugs. *Cancer Research* 58, 5315 (1998).
65. X. J. Cheng, J. C. Lin, Y. F. Ding, L. Zhu, J. Ye, and S. P. Tu, Survivin inhibitor YM155 suppresses gastric cancer xenograft growth in mice without affecting normal tissues. *Oncotarget* 7, 7096 (2016).
66. T. Nitta, H. Koike, T. Miyao, Y. Miyazawa, H. Kato, Y. Furuya, Y. Sekine, and K. Suzuki, YM155 reverses statin resistance in renal cancer by reducing expression of survivin. *Anticancer Research* 37, 75 (2017).
67. S. A. Stacker, C. Caesar, M. E. Baldwin, G. E. Thornton, R. A. Williams, R. Prevo, D. G. Jackson, S. Nishikawa, H. Kubo, and M. G. Achen, VEGF-D promotes the metastatic spread of tumor cells via the lymphatics. *Nature Medicine* 7, 186 (2001).
68. V. van Iterson, M. Leidenius, K. von Smitten, P. Bono, and P. Heikkila, VEGF-D in association with VEGFR-3 promotes nodal metastasis in human invasive lobular breast cancer. *American Journal of Clinical Pathology* 128, 759 (2007).
69. S. Juttner, C. Wissmann, T. Jons, M. Vieth, J. Hertel, S. Gretschel, P. M. Schlag, W. Kemmner, and M. Hocker, Vascular endothelial growth factor-D and its receptor VEGFR-3: Two novel independent prognostic markers in gastric adenocarcinoma. *Journal of Clinical Oncology: Official Journal of the American Society of Clinical Oncology* 24, 228 (2006).
70. B. Cong, X. Zhao, X. G. Zhao, X. P. Dong, and C. L. Peng, Relation of vascular endothelial growth factor-D expression to microvessel density, microlymphatic vessel density, and lymph-node metastasis of lung adenocarcinoma. *Zhonghua yi xue za zhi* 88, 2179 (2008).
71. M. Iida, T. Sasaki, and H. Komatani, Overexpression of Plk3 causes morphological change and cell growth suppression in Ras pathway-activated cells. *Journal of Biochemistry* 146, 501 (2009).
72. C. W. Conn, R. F. Hennigan, W. Dai, Y. Sanchez, and P. J. Stambrook, Incomplete cytokinesis and induction of apoptosis by overexpression of the mammalian polo-like kinase, Plk3. *Cancer Research* 60, 6826 (2000).

73. D. R. Croft and M. F. Olson, Transcriptional regulation of Rho GTPase signaling. *Transcription* 2, 211 **(2011)**.
74. M. Huang, J. B. Duhadaway, G. C. Prendergast, and L. D. Laury-Kleintop, RhoB regulates PDGFR-beta trafficking and signaling in vascular smooth muscle cells. *Arteriosclerosis, Thrombosis, and Vascular Biology* 27, 2597 **(2007)**.
75. G. C. Prendergast, Farnesyltransferase inhibitors define a role for RhoB in controlling neoplastic pathophysiology. *Histology and Histopathology* 16, 269 **(2001)**.
76. A. Basu and S. Haldar, The relationship between Bcl2, Bax and p53: Consequences for cell cycle progression and cell death. *Molecular Human Reproduction* 4, 1099 **(1998)**.
77. J. K. Brunelle and A. Letai, Control of mitochondrial apoptosis by the Bcl-2 family. *Journal of Cell Science* 122, 437 **(2009)**.
78. A. Sugimoto, R. R. Hozak, T. Nakashima, T. Nishimoto, and J. H. Rothman, dad-1, an endogenous programmed cell death suppressor in Caenorhabditis elegans and vertebrates. *The EMBO Journal* 14, 4434 **(1995)**.
79. J. Davoodi, M. H. Ghahremani, A. Es-Haghi, A. Mohammad-Gholi, and A. Mackenzie, Neuronal apoptosis inhibitory protein, NAIP, is an inhibitor of procaspase-9. *The International Journal of Biochemistry and Cell Biology* 42, 958 **(2010)**.
80. J. Chai, E. Shiozaki, S. M. Srinivasula, Q. Wu, P. Datta, E. S. Alnemri, and Y. Shi, Structural basis of caspase-7 inhibition by XIAP. *Cell* 104, 769 **(2001)**.
81. M. Paulsen, S. Ussat, M. Jakob, G. Scherer, I. Lepenies, S. Schutze, D. Kabelitz, and S. Adam-Klages, Interaction with XIAP prevents full caspase-3/-7 activation in proliferating human T lymphocytes. *European Journal of Immunology* 38, 1979 **(2008)**.
82. J. V. Falvo, A. V. Tsytsykova, and A. E. Goldfeld, Transcriptional control of the TNF gene. *Current Directions in Autoimmunity* 11, 27 **(2010)**.
83. M. Fotin-Mleczek, F. Henkler, A. Hausser, H. Glauner, D. Samel, A. Graness, P. Scheurich, D. Mauri, and H. Wajant, Tumor necrosis factor receptor-associated factor (TRAF) 1 regulates CD40-induced TRAF2-mediated NF-kappaB activation. *The Journal of Biological Chemistry* 279, 677 **(2004)**.